



HAL
open science

Structural and Functional Insights into *Saccharomyces cerevisiae* Tpa1, a Putative Prolylhydroxylase Influencing Translation Termination and Transcription

Julien Henri, Delphine Rispal, Emilie Bayart, Herman van Tilbeurgh,
Bertrand Séraphin, Marc Graille

► **To cite this version:**

Julien Henri, Delphine Rispal, Emilie Bayart, Herman van Tilbeurgh, Bertrand Séraphin, et al.. Structural and Functional Insights into *Saccharomyces cerevisiae* Tpa1, a Putative Prolylhydroxylase Influencing Translation Termination and Transcription. *Journal of Biological Chemistry*, 2010, 285 (40), pp.30767 - 30778. 10.1074/jbc.m110.106864 . hal-03298541

HAL Id: hal-03298541

<https://hal.science/hal-03298541>

Submitted on 23 Jul 2021

HAL is a multi-disciplinary open access archive for the deposit and dissemination of scientific research documents, whether they are published or not. The documents may come from teaching and research institutions in France or abroad, or from public or private research centers.

L'archive ouverte pluridisciplinaire **HAL**, est destinée au dépôt et à la diffusion de documents scientifiques de niveau recherche, publiés ou non, émanant des établissements d'enseignement et de recherche français ou étrangers, des laboratoires publics ou privés.

Structural and Functional Insights into *Saccharomyces cerevisiae* Tpa1, a Putative Prolylhydroxylase Influencing Translation Termination and Transcription^{*[5]}

Received for publication, January 22, 2010, and in revised form, June 17, 2010. Published, JBC Papers in Press, July 14, 2010, DOI 10.1074/jbc.M110.106864

Julien Henri^{‡1,2}, Delphine Rispal^{§¶1,2}, Emilie Bayart[§], Herman van Tilbeurgh^{‡3}, Bertrand Séraphin^{§¶3,4}, and Marc Graille^{‡2,5}

From the [‡]Institut de Biochimie et Biophysique Moléculaire et Cellulaire, CNRS UMR8619 Bat 430 Université Paris Sud, 91405 Orsay Cedex, France, the [§]Centre de Génétique Moléculaire, CNRS, 1 Avenue de la Terrasse, 91198 Gif-sur-Yvette Cedex, France, and the [¶]Institut de Génétique et de Biologie Moléculaire et Cellulaire, 1 rue Laurent Fries, BP 10142, 67404 Illkirch Cedex, France

Efficiency of translation termination relies on the specific recognition of the three stop codons by the eukaryotic translation termination factor eRF1. To date only a few proteins are known to be involved in translation termination in eukaryotes. *Saccharomyces cerevisiae* Tpa1, a largely conserved but uncharacterized protein, has been described to associate with a messenger ribonucleoprotein complex located at the 3' end of mRNAs that contains at least eRF1, eRF3, and Pab1. Deletion of the *TPA1* gene results in a decrease of translation termination efficacy and an increase in mRNAs half-lives and longer mRNA poly(A) tails. In parallel, *Schizosaccharomyces pombe* Ofd1, a Tpa1 ortholog, and its partner Nro1 have been implicated in the regulation of the stability of a transcription factor that regulates genes essential for the cell response to hypoxia. To gain insight into Tpa1/Ofd1 function, we have solved the crystal structure of *S. cerevisiae* Tpa1 protein. This protein is composed of two equivalent domains with the double-stranded β -helix fold. The N-terminal domain displays a highly conserved active site with strong similarities with prolyl-4-hydroxylases. Further functional studies show that the integrity of Tpa1 active site as well as the presence of Yor051c/Ett1 (the *S. cerevisiae* Nro1 ortholog) are essential for correct translation termination. In parallel, we show that Tpa1 represses the expression of genes regulated by Hap1, a transcription factor involved in the response to levels of heme and oxygen. Altogether, our results support that Tpa1 is a putative enzyme acting as an oxygen sensor and influencing several distinct regulatory pathways.

Protein synthesis is a complex process performed by ribosomes, translation factors, and amino-acyl tRNAs that act synergistically to translate mRNAs into corresponding proteins. The mechanism of translation of mRNAs into protein can be divided into three major steps; they are initiation, elongation, and termination. In eukaryotes, translation initiation relies on the formation of a stable closed-loop structure bringing the 5' m⁷G cap and the 3' poly(A) tail of a single mRNA in proximity and requires at least 11 initiation factors (1, 2). During elongation, the mRNA codon present in the ribosomal A site is recognized by a cognate amino-acyl tRNA associated with elongation factor 1A. The nascent polypeptide chain is then transferred from the tRNA present in the P-site to the amino acid of the A-site tRNA. Subsequently, elongation factor 2 induces translocation of peptidyl-tRNA from the A- to the P-site allowing the next elongation step to proceed. The entrance of one of the three stop codons (UAA, UAG, or UGA) in the A-site triggers translation termination. In contrast with other codons, stop codons are not recognized by cognate tRNAs but by proteins known as class I release factors (RF1⁶ and RF2 in bacteria and eRF1 in eukaryotes). These are also directly involved in the hydrolysis of the ester bond connecting the newly synthesized polypeptide chain to the tRNA located in the ribosomal P-site (3–5). The activity of class I RFs is stimulated by the class II RFs GTPases: RF3 in bacteria and eRF3 in eukaryotes (3–6). The eRF1 and eRF3 proteins form a stable complex in the absence of the ribosome (7, 8). The GTP hydrolysis activity of eRF3 is dependent on ribosome-bound eRF1 (9), but the eRF3 precise role remained obscure until recently. *In vitro* reconstitution of eukaryotic translation system indicated that binding of the eRF1·eRF3·GTP ternary complex to pre-termination complexes causes a structural rearrangement of the ribosome. This results in GTP hydrolysis by eRF3 followed by eRF1-induced hydrolysis of peptidyl-tRNA (6).

Translation termination relies on the efficient and specific recognition of stop codons (UGA, UAA, and UAG) by eRF1 despite the presence of near-cognate tRNAs (such as the tRNA^{Trp} that recognizes the UGG codon) that could induce

* This work was supported by La Ligue contre le Cancer "Equipe Labelisée 2008" and the CNRS. This work was also supported by the CNRS and Agence Nationale pour la Recherche Grant ANR-06-BLAN-0075-02 (to M. G.).

[5] The on-line version of this article (available at <http://www.jbc.org>) contains supplemental Table 1 and Figs. S1 and S2.

The atomic coordinates and structure factors (code 3MGU) have been deposited in the Protein Data Bank, Research Collaboratory for Structural Bioinformatics, Rutgers University, New Brunswick, NJ (<http://www.rcsb.org/>).

¹ Both authors contributed equally to this work.

² Recipients of Ph.D. fellowships from Université Paris Sud-11.

³ Supported by the European Union 6th Framework programs "3D-Repertoire" (LSHG-CT-2005-512028).

⁴ To whom correspondence may be addressed: IGBMC, 1 rue Laurent Fries, BP 10142, 67404 Illkirch Cedex, France. Tel.: 33-388653356; Fax: 33-388653200. E-mail: seraphin@igbmc.fr.

⁵ To whom correspondence may be addressed. Tel.: 33-169153157; Fax: 33-169853715. E-mail: marc.graille@u-psud.fr.

⁶ The abbreviations used are: RF, release factor; 2OG, 2-oxoglutarate; DSBH, double-stranded β -helix; HIF1 α , hypoxia-inducible transcription factor; CODD, C-terminal oxygen degradation domain; BMV, Brome mosaic virus; SREBP, sterol regulatory element-binding protein; SeMet, selenomethionine; r.m.s.d., root mean square deviation.

Structural and Functional Study of Tpa1, an O₂ Sensor

amino acid misincorporation and the synthesis of C-terminal extensions. The efficiency of stop codon recognition is primarily influenced by the stop codon itself and the first downstream nucleotide, commonly referred to as the tetranucleotide termination signal (10). Several *trans*-acting factors influencing the accuracy of this process have also been identified (11). Among these, the interaction of eRF3 with the poly(A)-binding protein (Pab1), which itself associates with the 3'-poly(A) tail present on almost all eukaryotic mRNAs, has been proposed to participate to normal translation termination and to mRNA stabilization (12, 13). The glutamine side chain from the strictly conserved GGQ motif from class I release factors has also been shown to be post-translationally modified both in prokaryotes and in eukaryotes, thereby affecting the efficiency of translation termination *in vivo*, at least in *Escherichia coli* (14–17). More recently, the deletion of the uncharacterized *Saccharomyces cerevisiae* open reading frame YER049W has been shown to result in increased readthrough of stop codons, longer poly(A) tails, and increased mRNAs half-lives (18). The YER049W gene product, named Tpa1, was co-immunoprecipitated with translation termination factors eRF1 and eRF3 as well as with the poly(A)-binding protein Pab1, suggesting that it could be part of a messenger ribonucleoprotein complex associated at the mRNA 3' end. Sequence analysis suggested that Tpa1 belongs to the 2-oxoglutarate-Fe(II) dioxygenase family (19). Dioxygenase enzymes catalyze oxidation reactions involving dioxygen and use 2-oxoglutarate (2OG) as co-substrate and ferrous ion (Fe²⁺) as cofactor. They are involved in various biological processes such as fatty acid metabolism, antibiotic biosynthesis, nucleic acid repair, collagen biosynthesis, histone Lys/Arg demethylation, and transcriptional regulation of the hypoxic response (20, 21). Recently, the Ofd1 protein, a Tpa1 ortholog from *Schizosaccharomyces pombe*, has been implicated with Nro1 (for negative regulator of Ofd1) in the regulation of low oxygen gene expression (22, 23). In *S. pombe*, the Sre1 transcription factor regulates the expression of genes involved in cholesterol and lipid biosynthesis (24, 25). Under low oxygen levels, the membrane-bound Sre1 protein is proteolytically cleaved, thus releasing its N-terminal transcription factor domain (26, 27). As a consequence, the transcription factor domain enters the nucleus and activates the expression of genes essential for hypoxic growth. In the absence of oxygen, the Ofd1 C-terminal domain was reported to interact with Nro1, and the Sre1 N-terminal domain is stabilized. In the presence of oxygen, the Ofd1 N-terminal dioxygenase domain would act as an oxygen sensor, activating its own C-terminal domain and preventing its interaction with Nro1, thus enhancing degradation of the Sre1 N-terminal domain.

Based on these two independent studies realized in *S. cerevisiae* and *S. pombe*, the precise Tpa1/Ofd1 function remains obscure. On the one hand, no clear ortholog of *S. pombe* Sre1 protein (homologous to human sterol regulatory element-binding protein (SREBP)) has been found in *S. cerevisiae*. On the other hand, a *S. cerevisiae* ortholog of Nro1 (Yor051c) does exist and was reported to interact with Tpa1 (28). Therefore, Tpa1/Ofd1 may have a role that is organism-dependent, and/or it may act on several distinct pathways. We present here the results of structural, biochemical, and genetic studies that

improve our understanding of the function of Tpa1, a protein conserved from fungi to human.

EXPERIMENTAL PROCEDURES

Cloning, Expression, and Purification of Tpa1—To overexpress Tpa1 in *E. coli*, its coding sequence was amplified from genomic DNA with oligonucleotides OBS2151 and OBS2152 (supplemental Table 1) and inserted in the BspE1 site of a modified pET vector, yielding pBS3077.

The protein has been expressed using *E. coli* Rosetta (DE3) pLysS strain (Novagen) at 23 °C in 2×YT medium (BIO101 Inc.) supplemented with kanamycin at 50 μg/ml. At A₆₀₀ = 0.8, the transcription of the plasmid was induced during 20 h by the addition of 50 μg/ml isopropyl 1-thio-β-D-galactopyranoside. Cells were harvested by centrifugation, resuspended in 35 ml of 20 mM Tris-HCl, pH 7.5, 200 mM NaCl, 5 mM β-mercaptoethanol (buffer A), and stored at –20 °C. Cell lysis was performed by sonication. The His-tagged protein was purified on a nickel-nitrilotriacetic acid column (Qiagen) followed by gel filtration chromatography on a Superdex™ 200 HL 16/60 column (GE Healthcare) equilibrated in buffer A.

Protein labeling with SeMet was conducted as described (29). The SeMet protein was purified using the same protocol as the native protein.

Size-exclusion Chromatography-Multiangle Laser Light Scattering Measurements—Sample injection, chromatography, and detection were carried out using a Triple Detector Array (TDA302) system coupled in line to a GPCmax chromatographic system (Viscotek). A sample of 100 μl of Tpa1 (6.2 mg/ml) was injected at a flow rate of 0.5 ml/min on a Superdex™ 200 HR 10/30 column (GE Healthcare) equilibrated in buffer A. Elution was followed by a UV-visible spectrophotometer, a differential refractometer, a 7° low angle light scattering detector, a 90° right angle light scattering detector, and a differential pressure viscometer. The data were collected and processed with the program OmniSEC (Viscotek). *M_r* was directly calculated from the absolute light scattering measurements. The *dn/dc* value (0.168) for Tpa1 has been determined experimentally using the refractive index at four different concentrations of Tpa1.

Structure Determination—Crystals of the native and SeMet protein were grown from a mixture in a 1:1 ratio of 15 mg/ml protein solution in buffer A and crystallization liquor containing 0.1 M Hepes, pH 7.5, 44% methylpentanediol, and 0.1 M Mg(NO₃)₂ at 18 °C over 2 months. The crystals were directly flash-cooled in liquid nitrogen.

Native crystal (crystal 1) diffracted to 2.8 Å of resolution on beam line ID14-EH2 at the European Synchrotron Radiation Facility (Grenoble, France). This crystal belongs to space group C222₁ with one molecule in the asymmetric unit (*a* = 81.2 Å, *b* = 104.8 Å, *c* = 205.6 Å, α = β = γ = 90°). SeMet crystals suffered from serious diffraction anisotropy (6 Å in one direction and 3.5–2.5 Å in the other one), but datasets could be recorded at the European Synchrotron Radiation Facility to 4 Å resolution on beam line ID23-EH1 (crystal 2) and 3.3 Å on beam line BM30A (crystal 3). The diffraction data were collected at the selenium edge (λ = 0.9796 Å). These crystals belong to

TABLE 1

	Native	SeMet 1	SeMet 2
Data collection			
Space group	C222 ₁	P2 ₁ 2 ₁ 2	P2 ₁ 2 ₁ 2
Unit cell parameters	<i>a</i> = 81.2 Å <i>b</i> = 104.8 Å <i>c</i> = 205.6 Å	<i>a</i> = 105.7 Å <i>b</i> = 168.2 Å <i>c</i> = 197.3 Å	<i>a</i> = 106.2 Å <i>b</i> = 169.0 Å <i>c</i> = 197.8 Å
Redundancy	3.58 (3.64)	4.64 (4.52)	3.82 (3.76)
Resolution range (Å)	50–2.8 (2.9–2.8)	50–3.4 (3.5–3.4)	50–3.7 (3.8–3.7)
Completeness (%)	97.0 (92.5)	97.0 (93.2)	98.1 (94.6)
<i>I</i> / σ (<i>I</i>)	6.76 (2.13)	8.29 (2.88)	6.13 (2.52)
<i>R</i> _{sym} (%)	15.3 (50.1)	16.2 (57.1)	19.1 (54.0)
Refinement			
Resolution (Å)	46.7–2.8		
<i>R</i> / <i>R</i> _{free} (%)	23.9/29.6		
Geometry statistics			
r.m.s.d. bonds (Å)	0.006		
r.m.s.d. angles (°)	1.077		
Average B-factor (Å ²)	52.10		
Ramachandran plot (Procheck)			
Most favored (%)	84.7		
Additionally allowed (%)	15.2		

space group P2₁2₁2₁ with four molecules in the asymmetric unit (*a* = 105.7 Å, *b* = 167.9 Å, *c* = 196.9 Å, $\alpha = \beta = \gamma = 90^\circ$).

The structure was determined by the single wavelength anomalous dispersion method using the anomalous signal of selenium (Se) atoms. Data were processed with the XDS package (30). The program SHELXD was used to find an initial set of 32 selenium sites (36 were expected according to the protein sequence and cell content) from the crystal 2 dataset in the 30–5.5 Å resolution range (31). Refinement of the selenium sites and phasing were carried out with the program SHARP using the SAD datasets collected on crystals 2 and 3 (32). Additional sites were included in the refinement after inspection of residual maps. The final substructure model comprises all expected selenium atoms. Phase refinement and extension were carried out via density modification and NCS averaging with the program RESOLVE (33). The experimental phases allowed initial automatic building by BUCCANEER (34). Iterative cycles of manual rebuilding using COOT (35) followed by refinement with PHENIX (36) led to a first almost-complete model. This model was then used for molecular replacement using native data collected on crystal 1 with MOLREP (37) and finally submitted to a new series of manual rebuilding with COOT and refinement with PHENIX. The statistics for data collection and refinement are summarized in Table 1. Due to the absence of electron density, the following regions were omitted from the final model: 1–25, 94–110, 269–275, 306–330, 455–459, 562–584, and 635–644. The atomic coordinates and structure factors have been deposited into the Brookhaven Protein Data Bank under accession numbers (3MGU).

Strains and Media—*S. cerevisiae* strains YJW618 (*MATa leu2-3,112 his3-11,15 trp1-1 ura3-1 ade1-14 PSI⁺*) and YJW619 (as YJW618 but *tpa1::LEU2*) were obtained from D. Bedwell (19). *YOR051C* was deleted in YJW618 and YJW619 with a *Candida glabrata* *HIS3* cassette amplified with OBS3866/OBS3867, giving strains BSY2236 and BSY2237, respectively. Cells were grown at 30 °C in standard media. Cell treatment with guanidine hydrochloride to test the role of the [*PSI*₊] factor was done as described previously (38).

The plasmid, pBS3820, containing the wild type *TPA1* gene was constructed by amplifying the *TPA1* ORF with upstream

and downstream sequences from genomic DNA using oligonucleotides OBS3527 and OBS3528 and inserting it between the BamHI and NotI sites of the pRS424 (*TRP1*, 2 μ) vector (39). The H159A/D161N allele was constructed by site-directed mutagenesis with primers OBS3687 and OBS3688 (supplemental Table 1) yielding pBS3793. Domain deletions pBS3794 and pBS3795 were constructed by PCR and cloning using oligonucleotides OBS3738–OBS3741. The TAP tag was introduced by cloning using oligonucleotides OBS3822–OBS3824, OBS3831, OBS3832, and OBS3844, yielding pBS3796–3799.

Stop Codon Readthrough Measurements—Yeast strains were transformed with reporters containing the coding sequences of the Renilla and firefly luciferase separated either by a stop codon (TAA) or a sense codon (CAA) as described (18). Three transformants were pooled and grown in selective liquid media to A₆₀₀ 0.5–0.8 for enzymatic assays. 10 μ l of yeast culture was used to measure the luminescence with the dual luciferase reporter assay reagent (Promega) in a Berthold luminometer. The percent readthrough is calculated from the ratio of firefly luciferase produced by the stop codon-containing construct to the firefly luciferase by the CAA-containing construct, normalized in each case to the level of Renilla luciferase produced in the same cells. Five biological experiments were performed with, in each case, technical duplicates. Differences reported were statistically significant (Mann-Whitney *U* test, 95% confidence interval).

β -Galactosidase Assay—Reporters, provided by B. Guiard (40), contained Hap1-driven UAS elements from the *CYC1* or *CYB2* genes, driving expression of β -galactosidase. Yeast strains were transformed with these reporters, and three transformants were pooled to perform β -galactosidase assays. Cells were grown to an A₆₀₀ of 0.5–0.8. 1 ml of culture is used. Assays were performed as previously described with three biological replicate and for each assay one technical duplicate (41).

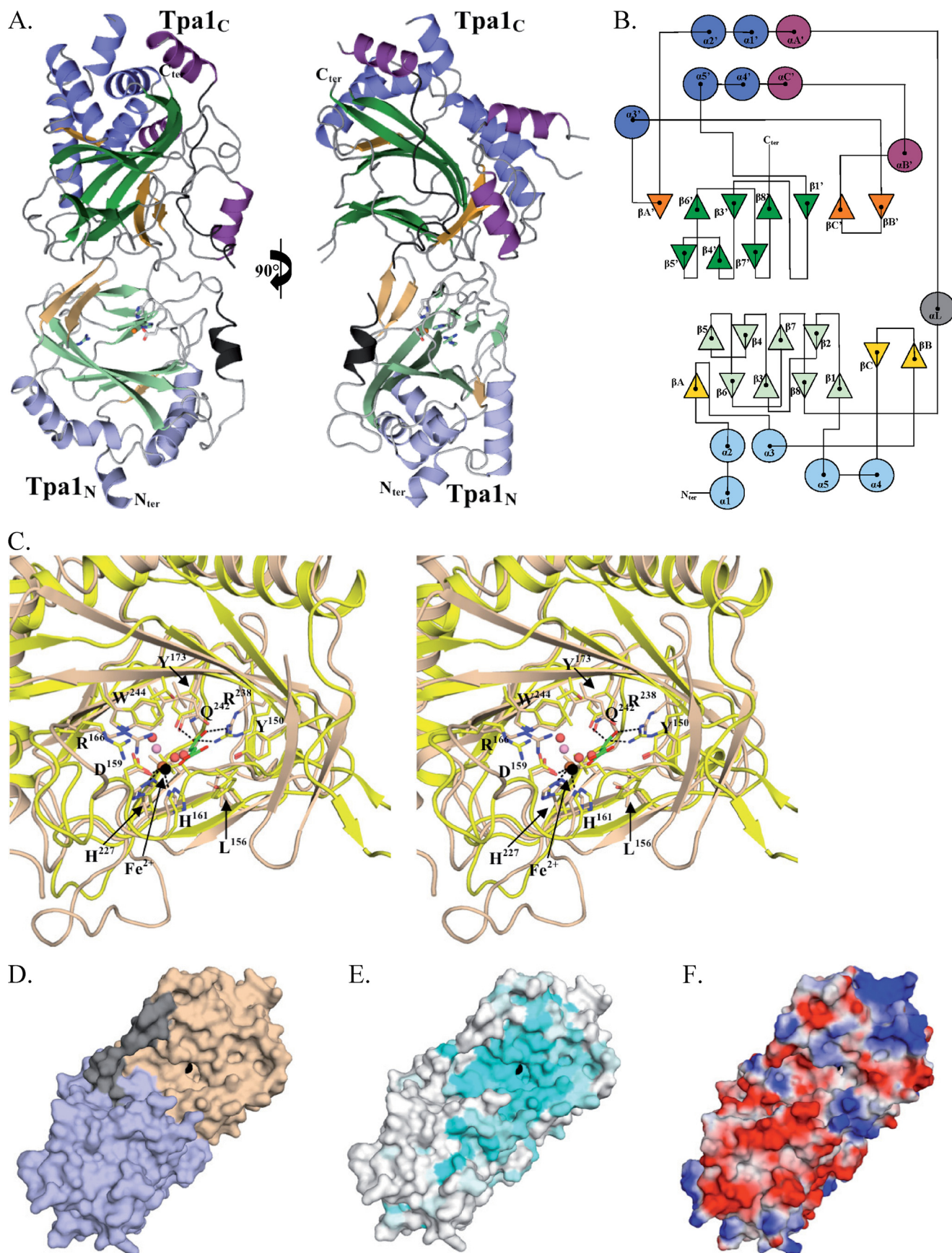
Protein Analyses—Proteins extracts (42) were fractionated on 8% SDS-PAGE, and TAP TAG proteins were detected with PAP (Sigma) and an ECL kit (GE Healthcare).

RESULTS

The structure of full-length *S. cerevisiae* Tpa1 has been solved using the single-wavelength anomalous diffraction signal of SeMet-substituted protein crystals and refined to 2.8 Å resolution using diffraction data from native protein crystals. The resulting density maps allowed us to rebuild 567 amino acids of 644. The missing residues correspond to the 25 N-terminal residues or the 9 C-terminal residues or belong to 5 loops for which no electron density was observed. The native protein crystallized in space group C222₁ with one molecule in the asymmetric unit, whereas the SeMet-labeled protein crystals grown under the same conditions belong to space group P2₁2₁2 with four Tpa1 copies in the asymmetric unit (one unit cell parameter is twice longer than for the native crystals). As a consequence, the crystal packing is identical between both crystal forms, and the Tpa1 protomers are organized as two identical dimers (buried surface 2000 Å²). This suggests that Tpa1 can form homodimers in solution (see below).

Tpa1 is composed of two stacked domains forming a cylinder of ~90 Å length and 45 Å diameter (Fig. 1A). The N-terminal domain (Tpa1_N) encompasses amino acids 26–260 (residues

Structural and Functional Study of Tpa1, an O₂ Sensor



Structural and Functional Study of Tpa1, an O₂ Sensor

1–25 are not visible in the electron density maps), whereas the C-terminal domain (Tpa1_C) encompasses amino acid 293–635 (residues 636–644 could not be modeled due to the lack of electron density). Both domains are packed together and connected by a linker (amino acids 261–292) that partially folds as α -helix.

The N-terminal Catalytic Domain—Sequence analysis has suggested that *S. cerevisiae* Tpa1 contains an N-terminal 2OG-Fe(II) dioxygenase domain from the double-stranded β -helix (DSBH) family based on the conservation of three characteristic motifs in the N-terminal part of the protein; a **HXD** dyad (where *X* is any amino acid) near the N terminus, a His toward the C terminus as well as an Arg or Lys farther downstream (19). Basically, the DSBH-fold consists of eight β -strands forming a β -sandwich structure composed of two four-stranded antiparallel sheets (21). The β -sandwich is partitioned between a minor (β -strands 2 if present, 7, 4, and 5) and a major sheet (β -strands 1, 8, 3, and 6) that very often contains additional strands. As proposed, the Tpa1_N domain adopts a DSBH-fold consisting of a β -sandwich of two antiparallel β -sheets with five α -helices packed onto the major sheet (Fig. 1B). This latter is composed of five β -strands (order 1, 8, 3, 6, and A). Two additional strands (β B and β C) are located at the entrance of the β -sandwich cavity.

The DSBH-fold is shared by a wide variety of Fe²⁺/2OG-dependent dioxygenases, and many crystal structures have been described for this architecture (21, 43). Structural alignments with Tpa1_N reveal similarity with prolyl-4-hydroxylases (r.m.s.d. of 2.3–2.5 Å over 150–170 C α atoms and 15–19% sequence identity), phytyl CoA dioxygenase (r.m.s.d. of 2.6 Å over 140 C α atoms and 15% sequence identity), DNA/RNA repair proteins AlkB/ABH3 (r.m.s.d. of 2.6 Å over 135–140 C α atoms and 10–15% sequence identity), and isopenicillin N synthase (r.m.s.d. of 2.7–2.9 Å over 150 C α atoms and 10% sequence identity). However, the closest structural homolog is human PHD2_{cat}, a prolyl-4-hydroxylase that acts as an oxygen-sensing component and post-translationally hydroxylates the hypoxia-inducible transcription factor HIF1 α in the presence of oxygen, thus leading to its degradation by the proteasome (r.m.s.d. of 2.5 Å over 153 C α atoms and 19% sequence identity (44)). Analysis of the amino acid side chains strictly conserved between Tpa1_N and PHD2_{cat} reveals that most are clustered within the cavity located between both β -sheets that corresponds to PHD2_{cat} enzyme active site (Fig. 1C). First of all, the **HXD...H** triad (positions 159, 161, and 227 in Tpa1, respectively) superposes perfectly with the characteristic **HXD...H** Fe²⁺ binding motif observed in PHD2_{cat}. The ¹⁵⁹HXD¹⁶¹ dyad is located within the loop connecting strands β 2 and β 3, whereas the second histidine (His²²⁷) originates from strand β 7. In typical DSBH enzymes, these three residues form a triad, leaving three coordination sites on the octahedral Fe(II) center for the binding of 2OG and dioxygen. During refinement, a

strong residual electron density peak was observed in close proximity to His¹⁵⁹, Asp¹⁶¹, and His²²⁷ of Tpa1, exactly at the position corresponding to the iron atom in PHD2_{cat} structure. Element analysis confirmed the presence of iron in the protein samples (ratio 1 iron atom for 2 Tpa1; data not shown). This metal is present at the entrance of a highly conserved cavity known to bind the 2OG co-substrate. All but two residues forming the 2OG binding pocket are strictly conserved between Tpa1_N and PHD2_{cat} (Fig. 1C, differences are Leu¹⁵⁶ and Gln²⁴² in Tpa1_N versus Tyr³¹⁰ and Thr³⁸⁷ in PHD2_{cat}). At the bottom of this cavity, the positively charged side chains from Arg²³⁸ from β 8 as well as Tyr¹⁷³ are well positioned to interact with the carboxyl side chain of the 2OG co-substrate. Similarly, the side chains from Tyr¹⁵⁰, Ile¹⁷¹, Leu¹⁸⁹, and Val²²⁹ of Tpa1_N form the wall of the 2OG binding site and structurally match with identical residues from PHD2_{cat}. Altogether, these elements strongly suggest that the Tpa1_N domain displays a putative active site configuration that is close to that from PHD2_{cat}.

Further inspection of amino acid sequences of the Tpa1/Ofd1 family clearly shows that the iron atom is located in the middle of a highly conserved groove delineated by side chains from Asp¹⁴⁴, Ser¹⁴⁶, Asp¹⁶⁰, Ile¹⁶³, and Arg¹⁶⁶ on one side and from the β -hairpin made by strands β B and β C (Lys⁸², Asp⁸⁶, Ile⁸⁷, Tyr⁸⁸, and Gln⁹²) on the other side (Fig. 1, D–E). This groove might be extended by residues 94–102 (connecting strand β C to helix α 4), which are well conserved in fungi but undefined in electron density maps and, hence, absent from the final model. It is very likely that this loop will become ordered upon substrate binding. In addition, the rather negative electrostatic potential of this crevice suggests that it could interact with a molecule or peptide containing positive charges (Fig. 1F). In summary, the strong structural similarity between Tpa1_N and human HIF prolyl-4-hydroxylase combined with the characteristics of the substrate binding groove suggest that Tpa1_N has a prolyl-4-hydroxylase activity on Pro and Arg/Lys-containing peptides that remains to be identified.

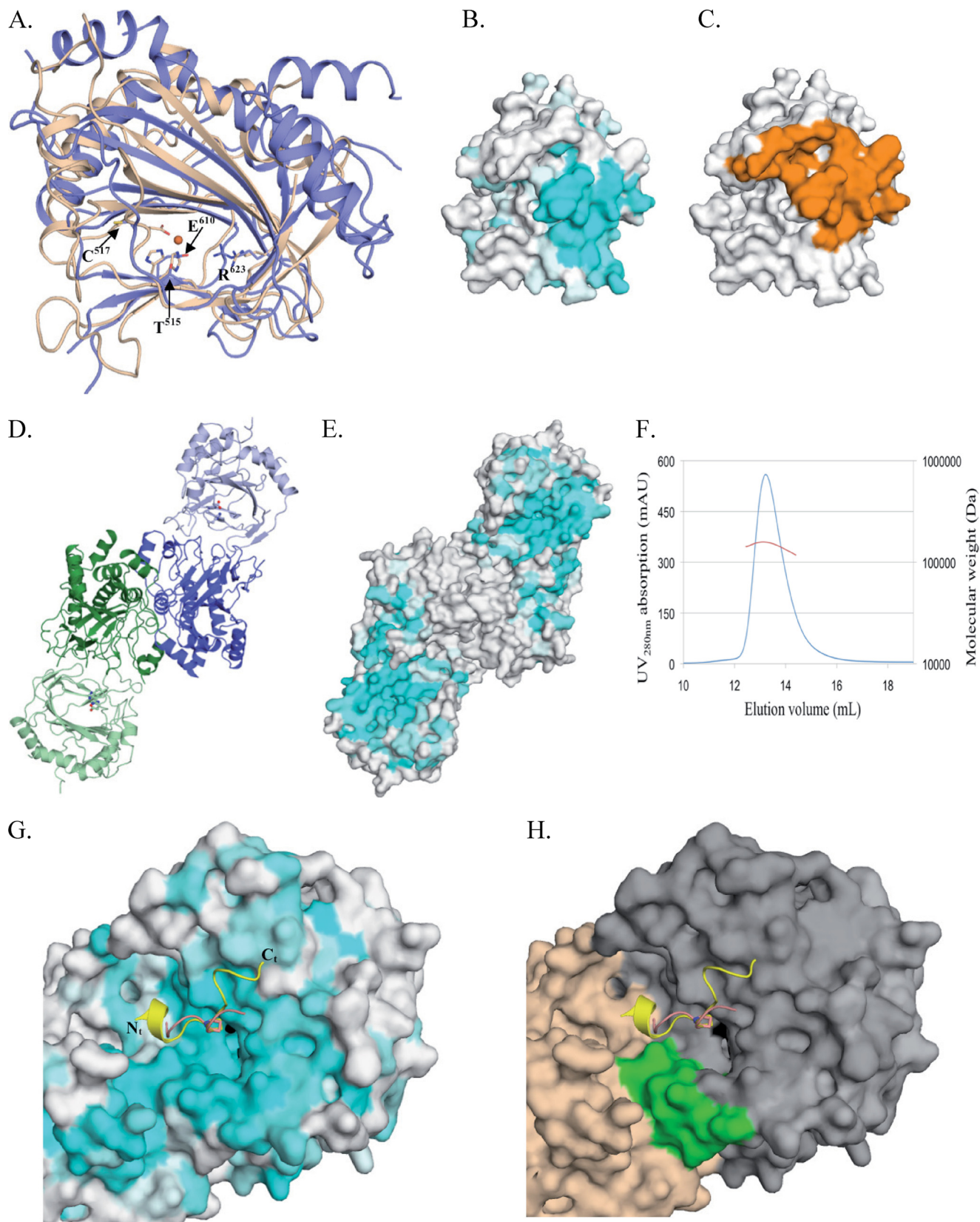
The C-terminal Domain and Its Association with Tpa1_N—Contrary to the Tpa1_N domain, amino acid sequence analysis did not provide convincing predictions for the three-dimensional structure of the Tpa1_C domain. Unexpectedly, this domain (residues 293–635) adopts a DSBH very similar to Tpa1_N (r.m.s.d. of 2.5 Å over 153 C α atoms despite only 13% sequence identity; Fig. 2A), suggesting an internal duplication event. The minor sheet of Tpa1_C is only made of three strands (β 7', 4', and 5') as the antiparallel hydrogen bond pairing of residues corresponding to strand β 2' and the neighboring strand β 7' are not maintained (Fig. 1, A and B). The major sheet is composed of seven antiparallel β strands (order A', 6', 3', 8', 1', C', and B'). Seven of the eight α -helices are packed against one face of the major sheet. Two helices (α A' and α B') are specific of this domain, whereas the remaining five (α 1' to α 5') are structural matches of the corresponding helices (α 1 to α 5)

FIGURE 1. *S. cerevisiae* Tpa1 structure. A, a ribbon representation of the Tpa1 protein is shown. B, a topology diagram is shown. The same color code as in panel A is used. C, a stereo view of Tpa1_N active site (light brown) superposed on PHD2_{cat} (yellow) is shown. The 2OG co-substrate has been modeled into the active site cavity by superposing the structure of a DSBH protein obtained in the presence of 2OG onto the Tpa1_N domain. Black and red spheres depict the iron atom and water molecules observed in the crystal structure, respectively. D, a surface representation of the Tpa1 protein is shown. Tpa1_N (wheat) and Tpa1_C (slate) are joined by a linker (gray). The iron atom is represented as a black sphere. E, a surface representation of residue conservation mapped at the surface of Tpa1 is shown. Coloring is from blue (highly conserved) to gray (low conservation). F, representation of electrostatic potential at the Tpa1 surface is shown.

Structural and Functional Study of Tpa1, an O₂ Sensor

from Tpa1_N. Despite its structural resemblance with Tpa1_N, the HXD...H catalytic triad is absent in Tpa1_C and is replaced by residues Thr⁵¹⁵, Cys⁵¹⁷, and Glu⁶¹⁰, which are not conserved

in Tpa1 orthologs (Fig. 2A and supplemental Fig. S1). In addition, the cavity of the Tpa1_C domain that corresponds to the active site in enzymes with a DSBH-fold is not lined by con-



served residues and is largely occluded by the linker region (residues 261–290) connecting both Tpa1 domains. Altogether, these elements argue that this domain is very unlikely to be associated with any enzymatic activity.

Tpa1_C has a large and highly conserved surface area that mainly contacts Tpa1_N domain (buried surface area of 1200 Å²; Fig. 2, *B* and *C*) and, hence, is not accessible. Contrary to Tpa1_C, the region from Tpa1_N engaged in interdomain interaction does not display significant sequence conservation. Both domains interact via orthogonal packing of their minor sheets (Fig. 1, *A* and *B*). This interaction positions the α-helical layers from both domains at the opposite sides of Tpa1. Tpa1_C is located below the entrance of the Tpa1_N active site and contributes to the formation of the conserved groove that runs across the Tpa1_N active site (Fig. 1, *D* and *E*). In addition, one face of Tpa1_C displays a negative electrostatic potential and is juxtaposed to the Tpa1_N conserved and negatively charged groove (Fig. 1*F*). This results in a large surface with negative potential that could be implicated in binding to a positively charged partner.

As stated above, analysis of the crystal packing reveals a tightly packed crystallographic dimer that buries 2000 Å² surface area, suggesting that Tpa1 forms dimers (Fig. 2, *D* and *E*). Dimer formation occurs between Tpa1_C domains and is mediated by poorly conserved residues from helices αA', α1', αC', α4', and α5', strand β1', and from the loops connecting α-helix to αA', αB' to αC', and β1' to β2'. The core of this interface is mainly hydrophobic, with some polar residues involved in its periphery. Analysis of the quaternary structure of Tpa1 in solution using size exclusion chromatography coupled online to a triple detection array (Viscotek) indicated a molecular mass of 143.3 kDa close to the value expected for the homodimer (150 kDa compared with 75 kDa for the monomer, Fig. 2*F*). The presence of Tpa1 homodimers *in vivo* remains to be determined. However, it is noteworthy that among the three residues from *S. cerevisiae* Tpa1 that have been identified by in-depth phosphoproteome analysis (45), one (Ser²⁹³) is located within a loop (connection between α-helix to αA') involved in this homodimeric interface. In our structure, this residue is not modified, but the protein has been produced in *E. coli*. Hence, we cannot exclude that the phosphorylation of Ser²⁹³ from Tpa1 will affect its quaternary structure and potentially its function.

To our knowledge this is the first example of a Fe(II)-2OG dioxygenase family with two DSBH domains in tandem. Cupin superfamily members (phosphomannose isomerase (46), oxalate decarboxylase (47), quercetin-2,3-dioxygenase (48), and the human transcription cofactor pirin (49)) also have repeated DSBH domains, but they are not 2OG-dependent enzymes.

Tpa1 differs from these proteins as Tpa1 domains are independent, whereas in pirin and related proteins, the domains are connected to each other by a strand-swapping mechanism; the N-terminal fragment contributing a β-strand to the C-terminal domain and vice versa.

Modeling of Tpa1 Bound to a “Substrate” Peptide—The strong structural similarity of Tpa1 with prolyl-4-hydroxylases suggests Tpa1 is an enzyme that post-translationally modifies proline residues in the presence of oxygen. Among these enzymes, some display broad substrate specificity as exemplified by collagen and algal prolyl-4-hydroxylases that modify the central proline of the X-Pro-Gly motif at several positions within collagen and proteins from the lumen of plant endoplasmic reticulum (50, 51). On the contrary, the human HIF1α prolyl-4-hydroxylase (PHD2 or EGLN1) selectively modifies Pro⁵⁶⁴ from HIF1α in the presence of oxygen, thereby leading to its degradation by the proteasome (52). Very recently, the mode of substrate binding to prolyl-4-hydroxylases was revealed by two high resolution crystal structures. The first one corresponds to the complex between algal prolyl-4-hydroxylase bound to a peptide corresponding to the (Ser-Pro)₅ motif (r.m.s.d. with Tpa1_N of 2.4 Å over 152 Cα atoms, 15% sequence identity (53)). The second is the crystal structure of PHD2_{cat} in complex with a 19-residues peptide (region 556–574 containing the targeted Pro⁵⁶⁴) from the C-terminal oxygen degradation domain (CODD) from HIF1α (r.m.s.d. with Tpa1_N of 2.5 Å over 170 Cα atoms, 19% sequence identity (54)). The CODD peptide binds in an extended form to a well defined cleft of the PHD2_{cat} active site. Using these complexes as templates, we modeled peptides within the Tpa1_N putative active site (Fig. 2*G*). In both models (with the exception of the C-terminal part of the CODD peptide), no major steric hindrance between the peptides and Tpa1 was observed. The peptides fit into the highly conserved long groove containing the putative Tpa1_N active site, and the hydroxylated proline is positioned close to the metal from the active site (distance between the Pro C4 atoms and the iron atom ≈ 4–5 Å). In both cases, the peptides have the same directionality within the active site groove (*i.e.* the N-terminal extremity from both peptides is located at the same end of the groove). The main difference between the Tpa1-peptide model structure and the prolyl-4-hydroxylase-substrate peptide complexes resides in the conformation of the β-hairpin made by strands βB and βC. In Tpa1, this region (residues 81–91) is in an open conformation and forms one side of the conserved groove (Fig. 2*H*). It is also engaged in a large interaction with Tpa1_C. In the PHD2_{cat} apo-structure, this region has an open conformation as observed for Tpa1_N, whereas upon CODD peptide binding, it folds back onto the substrate and clamps Pro⁵⁶⁴ in the active site. This region

FIGURE 2. *A*, a stereo view representation of the superposition of Tpa1_N (light brown) on Tpa1_C (blue) is shown. *B*, a surface representation of residue conservation mapped at the surface of the Tpa1_C domain is shown. Coloring is from blue (highly conserved) to gray (low conservation). *C*, Tpa1_C interacting surface with Tpa1_N is shown. *D*, a ribbon representation of the Tpa1 homodimer observed in the crystal is shown. One monomer is shown in blue, and the other one is in green. Tpa1_N and Tpa1_C are in light and dark colors, respectively. *E*, surface representation of residue conservation mapped at the surface of Tpa1 homodimer is shown (same color code as Fig. 2*A*). *F*, size-exclusion chromatography as followed by a triple detector array of Tpa1 is shown. For clarity only, the UV absorption (280 nm) for the eluted sample (left y axis) and molecular mass calculated from light scattering (right y axis, logarithmic scale) are shown. *GAU*, milliabsorbance units. *G*, shown is a surface representation of Tpa1 active site (same color code as Fig. 2*A*) with the HIFα CODD (yellow) and (Ser-Pro)₅ (pink) peptides shown in ribbon. The hydroxylated proline is shown in sticks. The iron atom is shown as a black sphere. *H*, the representation is the same as panel *G*. Tpa1_N and Tpa1_C are colored gray and beige, respectively. The βB-βC β-hairpin is shown in green.

Structural and Functional Study of Tpa1, an O₂ Sensor

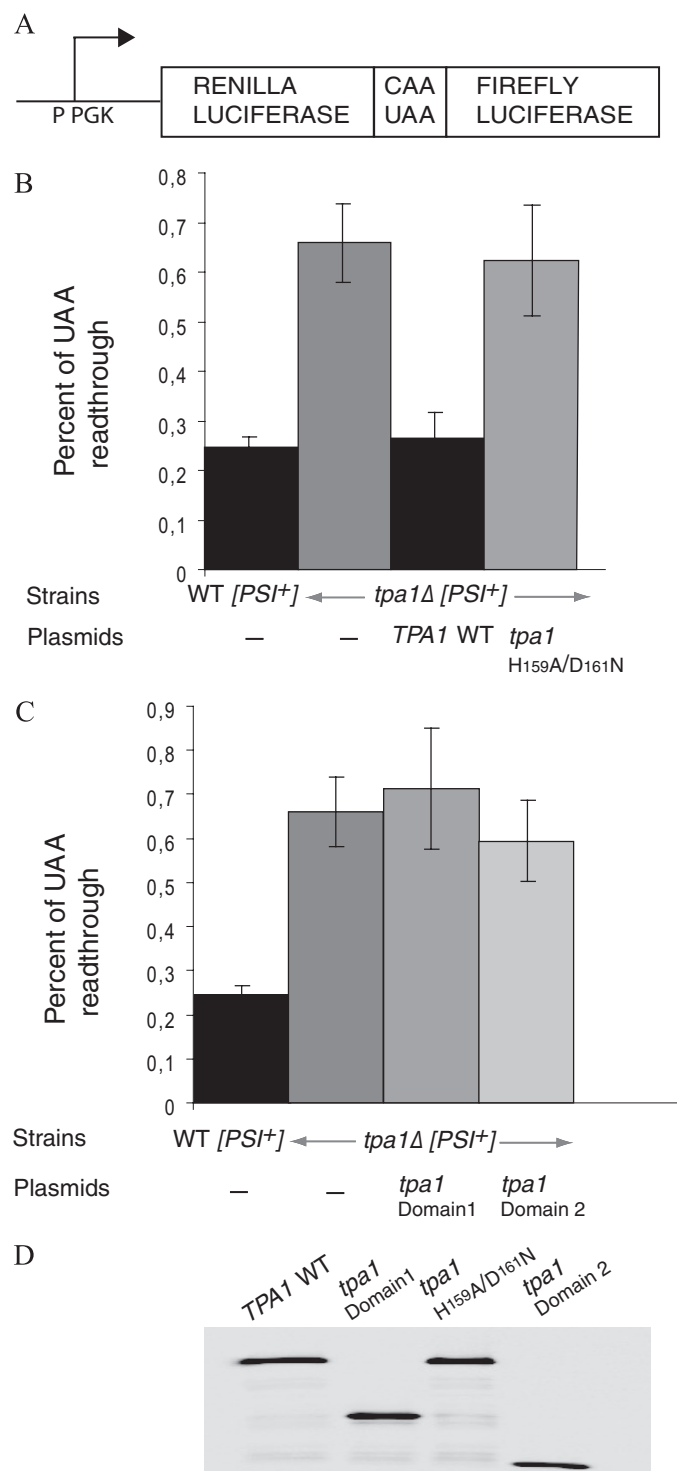


FIGURE 3. Requirement of both Tpa1 domains and of conserved residues in its putative catalytic center for stop codon readthrough. *A*, shown is the structure of the reporter used to measure stop codon readthrough. Synthesis of mRNAs encoding both the Renilla and firefly luciferases is driven by a *P_{gk-1}* promoter (*P_{PGK}*). The two ORFs are separated either by a CAA codon encoding glutamine or by the UAA stop codon. Percent of stop codon readthrough is calculated as the ratio of firefly luciferase to Renilla luciferase for the stop codon-containing construct divided by the ratio of firefly luciferase to Renilla luciferase for the construct encoding glutamine $\times 100$. *B*, the percent of UAA readthrough in wild type *PSI⁺* cells (YJW618 strain transformed with the empty vector) or in the isogenic strain deleted for *TPA1* (YJW619 strain) carrying either an empty vector, a plasmid encoding wild type *TPA1* gene, or the Tpa1 H159A/D161N mutant is plotted. S.D. from five experiments are indicated. *C*, the experiments were the same as in *B*, except that plasmids encod-

undergoes the largest conformational changes upon substrate binding (54). Similar conformational changes occur upon peptide binding for the corresponding β -hairpin of algal prolyl-4-hydroxylase (53). Whether rearrangements of the Tpa1 β -hairpin take place upon substrate binding is hard to predict in the absence of any information on Tpa1 substrates. Rearrangements of this β -hairpin very likely would affect the interface between both Tpa1 domains. This would result in a different orientation of these domains, thereby exposing to solvent part of the highly conserved region of Tpa1_C that interacts with Tpa1_N.

Mutation of Conserved Residues in the Putative Tpa1 Catalytic Site Promote Stop Codon Readthrough—The implication of Tpa1 in translational readthrough, mRNA decay, and poly(A) tail length control (18) offered a possibility to test whether the putative catalytic residues of Tpa1 are important for its function. Similarly, the two domains of Odf1, the *S. pombe* homolog of Tpa1, were shown to have different functions in the oxygen-dependent degradation of the active form of the Sre1 transcription factor (22). It was, thus, also interesting to test the role(s) of the two domains of Tpa1. For this purpose, we concentrated on the level of stop codon readthrough using reporter plasmids encoding two luciferases (Renilla and firefly) separated either by a UAA stop codon or by CAA encoding glutamine (Fig. 3*A* (18)). These constructs were introduced in a wild type yeast strain or a strain deleted for *TPA1* (*tpa1Δ*). In addition, these plasmids were introduced in the *tpa1Δ* strain simultaneously with a plasmid encoding either the wild type *TPA1* gene or mutant alleles. Stop codon readthrough was first assayed by measuring the relative activities of the two types of luciferase produced by these cells, with 100% readthrough being taken as the ratio observed for the construct with a CAA codon. Consistent with the previous report (18), deletion of the *TPA1* gene resulted in a roughly 3-fold increase of the readthrough of the UAA stop codon (Fig. 3, *B* and *C*). Introduction of a plasmid-borne copy of the wild type *TPA1* gene essentially corrected this defect, restoring low readthrough of the stop codon (Fig. 3*B*). To inactivate the catalytic activity of Tpa1, we substituted simultaneously His¹⁵⁹ in alanine and Asp¹⁶¹ in asparagine. Substitution of either one of the equivalent residues in the related protein hABH3 totally abrogates its DNA repair activity (55). Interestingly, a plasmid encoding the H159A/D161N allele of the *TPA1* gene failed to complement the *tpa1Δ* strain in the stop codon readthrough assay (Fig. 3*B*). The effect was not specific for luciferase reporter, as it was also observed by scoring the cell color and growth on media without adenine that report expression of the UGA-containing *ade1-14* allele (supplemental Fig. S2). Similarly, plasmids encoding either the Tpa1_N or Tpa1_C domains failed to restore translation termination efficiency to a wild type level (Fig. 3*C* and supplemental Fig. S2). To exclude that mutation of the putative Tpa1 catalytic center or deletion of one or the other of its domains destabilized the resulting protein (which would have provided a straightforward explanation for their apparent lack of activity),

ing either Tpa1_N or Tpa1_C were used. *D*, shown is Western blot analysis of total cellular protein extracted from cells expressing Tpa1-TAP, Tpa1_N-TAP, Tpa1-H159A/D161N-TAP, or Tpa1_C-TAP.

Structural and Functional Study of Tpa1, an O₂ Sensor

the levels of the wild type and mutant proteins fused to an epitope tag were measured by Western blot (Fig. 3D). This demonstrated that the three mutants were expressed to a level similar to the wild type protein and were equally stable (even though a slightly lower level of the protein containing Tpa1_C alone was detected). We conclude that the observed phenotypes do not result from lack of Tpa1. Thus, it appears that both domains of Tpa1 as well as its putative catalytic activity are required to favor stop codon recognition in yeast cells.

Ett1, the *S. cerevisiae* Nro1 Homolog Also Affects Stop Codon Readthrough—Recently, a factor, Nro1, was shown to interact with Ofd1 in *S. pombe* and proposed to inhibit the ability of Ofd1 to degrade the active form of the Sre1 transcription factor (23). It is noteworthy that, using TAP purification (56), the Nro1 homolog in *S. cerevisiae*, Yor051c, was independently found to interact with Tpa1 (homologous to Ofd1) (28). To strengthen the parallel between these distantly related yeast species, we constructed a *S. cerevisiae* strain lacking the *YOR051C* gene and a strain in which both the *TPA1* and *YOR051C* genes had been simultaneously inactivated. Both strains were transformed with the reporter plasmids, and the level of stop codon trans-reading was assayed (Fig. 4A). This demonstrated that, similarly to *TPA1*, *YOR051C* gene deletion increased stop codon readthrough. Moreover, the effects of *TPA1* and *YOR051C* deletions were not additive, suggesting that they act in the same pathway. Altogether, these data support the idea that, as for Ofd1 and Nro1 in *S. pombe*, Yor051c and Tpa1 activities are linked in *S. cerevisiae*. However, although Nro1 was suggested to antagonize Ofd1 activity, we observed similar, rather than opposite effects of Tpa1 and Yor051c proteins on stop codon trans-reading. Due to this difference with *S. pombe* Nro1, we therefore propose to name the *S. cerevisiae* *YOR051C* gene product Ett1 for enhancer of translation termination 1.

Tpa1 has already been shown to control stop codon readthrough independently of the status of the *PSI* factor that varies according to the aggregation state of the eRF3 proteins (18). To ascertain that this is the case and test whether this holds true for Ett1, we cured *PSI*⁺ cells by guanidine hydrochloride treatment and assayed the expression of *ade1-14* through accumulation of derived red pigment and growth in media lacking adenine in *PSI*⁺ and *PSI*⁻ strains carrying the *TPA1* or *ETT1* deletion or wild type as a control (Fig. 4B). Deletion of *TPA1* and *ETT1* genes enhanced stop codon readthrough in both *PSI*⁺ and *PSI*⁻ contexts. We conclude that the effect of these proteins on stop codon readthrough does not occur exclusively through control of eRF3 aggregation. Quantitatively, for luciferase production, accumulation of red pigment, and growth on media without adenine, stop codon readthrough was lower in the *ett1Δ* strain compared with the *tpa1Δ* strain (Fig. 4, A and B). Both experiments reflect a general effect of Tpa1 and Ett1 on translation termination.

Tpa1 Deletion Affects Expression of Some Genes Responsive to Oxygen Concentration—Because Ofd1 regulates expression of a transcription factor mediating the response to oxygen concentration in *S. pombe* (22) and given the structural evidence implicating Tpa1 in an oxygen-dependent reaction, we asked whether expression of genes known to be affected by

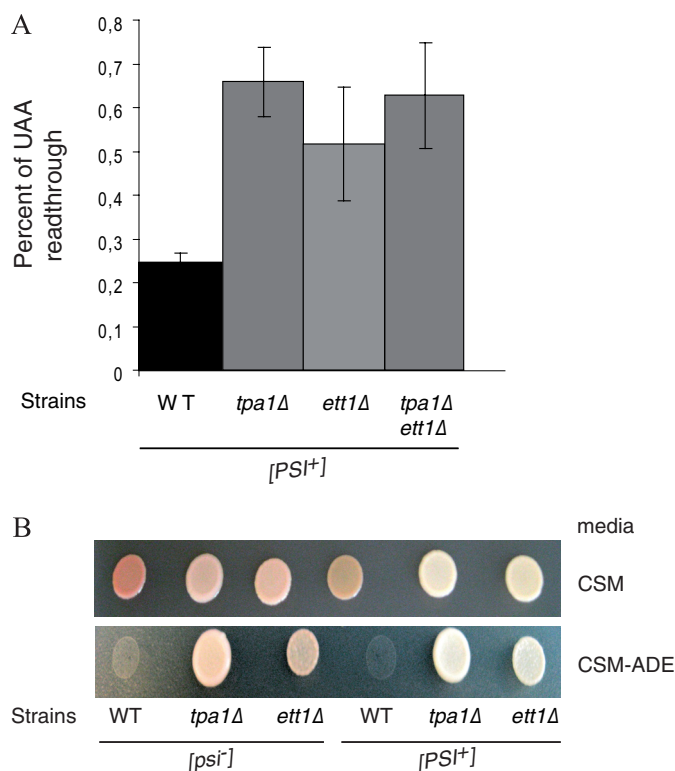


FIGURE 4. Ett1 affects stop codon readthrough. A, readthrough of the stop codon in the wild type strain (YJW618 strain), in the isogenic strain lacking either *TPA1* or *ETT1*, or in both genes was measured as described in Fig. 3. B, increased readthrough of the UGA codon present in the *ade1-14* allele in strains lacking *TPA1*, *ETT1* is demonstrated by reduced accumulation of the red pigment in these cells on complete synthetic media (CSM) and proportional increased growth on complete synthetic media without adenine (CSM-ADE). Readthrough is decreased in *PSI*⁻ cells (obtained after treatment with guanidine hydrochloride), but the effect of *TPA1* and *ETT1* deletion is still clearly detectable, indicating that Tpa1 and Ett1 do not act through the control of eRF3 aggregation. This is consistent with previously reported results (18). For this assay equivalent numbers of cells of the yeast strains of the indicated genotype were grown on complete synthetic media (CSM) or CSM without adenine (CSM-ADE) media for 3 days at 30 °C (using this strain background, at this time point, suppression of the *ade1-14* mutation by *PSI*⁺ on these media was sufficiently limited to allow scoring of the suppression of *ade1-14*, resulting from the deletion of *TPA1* or *ETT1*). Note that both in *PSI*⁺ and *PSI*⁻ context, deletion of *ETT1* had a lower effect on readthrough using both assays compared with the deletion of *TPA1*.

oxygen concentration is influenced by the presence of Tpa1. Genes under the control of Mga2 (57) and Hap1 (58) were tested for this purpose. Although we did not detect a significant difference of expression of a β -galactosidase reporter driven by a Mga2-sensitive promoter between wild type and *tpa1Δ* strains (data not shown), we observed significant changes of expression of reporters in which transcription was driven by activating sequences binding Hap1, such as the *CYC1* UAS1 and the *CYB2* UAS1 (Fig. 5). In both cases, β -galactosidase levels were increased roughly 4-fold in the *tpa1Δ* strain compared with the wild type isogenic control. Because Mga2-dependent promoters were not affected in this assay, this result suggests that Tpa1 represses specifically Hap1 activity by an unknown mechanism.

DISCUSSION

In eukaryotes, the detection of the three mRNA stop codons in the A-site of the ribosome is ensured by two interacting

Structural and Functional Study of Tpa1, an O₂ Sensor

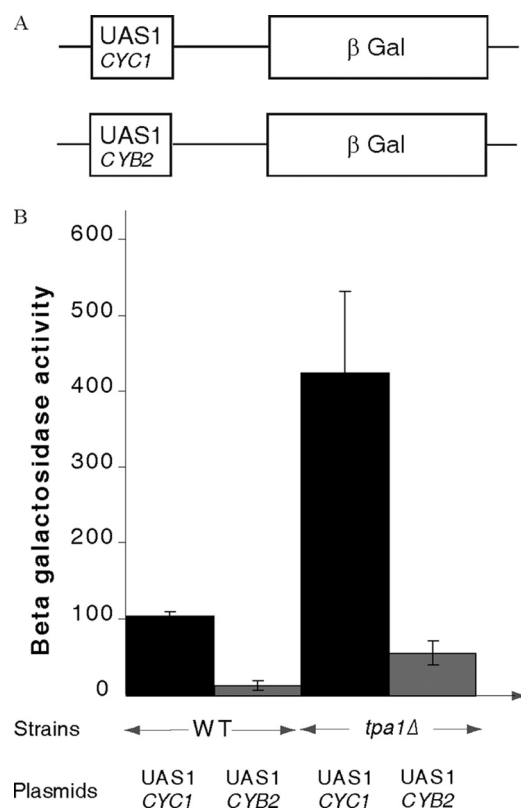


FIGURE 5. Tpa1 is required for full activity of Hap1-dependent promoters. *A*, structure of the two reporters used for this assay is shown. *B*, the levels of β -galactosidase activity measured for the reporter with the *CYC1* UAS1 or the *CYB2* UAS1 in either the wild type or the *tpa1*Δ strains are plotted with the standard deviation from three experiments.

translation termination factors: eRF1 and eRF3. Upon binding to the ribosome, this complex triggers hydrolysis of the ester bond connecting the polypeptide chain to the tRNA located in the ribosomal P-site, thereby releasing the newly synthesized protein. Accurate translation termination requires efficient recognition of stop codons (UAA, UAG, or UGA) by eRF1. Tpa1, a previously uncharacterized protein was recently shown to affect this process (18). In parallel, Ofd1, the *S. pombe* homolog of Tpa1, was implicated in the oxygen-dependent regulation of Sre1, the sterol regulatory element-binding protein from fission yeast (22). Due to the fact that independent studies in different organisms on the role of the Tpa1/Ofd1 orthologs yielded non-overlapping results, no unifying view on the Tpa1/Ofd1 system has yet been proposed. To progress on this issue, we initiated a structure-based functional analysis of *S. cerevisiae* Tpa1. We have solved the crystal structure of Tpa1 to 2.8 Å resolution. As suggested for *S. pombe* Ofd1, Tpa1 is composed of two domains. Interestingly, both domains adopt the same DSBH-fold found in 2OG-Fe(II) dioxygenases (Figs. 1, *A* and *B*, and 2*A* (43)). The N-terminal domain (Tpa1_N) harbors the catalytic residues (HXD...H triad) present in all members of this class of enzymes (Figs. 1*C* and 2*A*), whereas they are absent in the structurally very similar C-terminal domain. The three invariant residues are localized in the middle of a highly conserved groove of the N-terminal domain (Fig. 1*E*). The conservation of both folding and catalytically important residues between Tpa1 and prolyl-4-hydroxylases (such as human PHD2 and algal prolyl-4-

hydroxylase (44, 53) Fig. 1*C*) strongly suggests that Tpa1 possesses a prolyl-4-hydroxylase enzymatic activity.

Tpa1 and Ett1 Are Involved in Correct Translation Termination—We further investigated the involvement of Tpa1 in the control of stop codon readthrough, poly(A) tail length and mRNA stability (18). In our hands, we were not able to detect significant effects of Tpa1 deletion on poly(A) tail length and mRNA stability. However, consistent with the previous results of Keeling *et al.* (18), the deletion of *TPA1* gene resulted in a roughly 3-fold increase of the readthrough of the UAA stop codon (Fig. 3, *B* and *C*). We also demonstrated that this effect was not gene-specific as *tpa1*Δ partly suppressed the *ade1-14* (UGA stop codon) mutation both for growth in media lacking adenine and for the resulting accumulation of the red pigment (Fig. 4*B*). Wild type levels of stop codon readthrough were restored by transformation of the *tpa1*Δ strain with a plasmid encoding wild type Tpa1. Next, we tested whether the Tpa1 active site is involved in translation termination efficiency by replacing the invariant HXD motif from the triad involved in metal binding by the AXN sequence. This mutant did not complement the *tpa1*Δ to restore translation termination efficiency, proving that the integrity of Tpa1 putative active site is necessary for this process, at least at UAA and UGA stop codons. Because Hughes and Espenshade (22) suggested that the N-terminal domain of Ofd1 regulates, in an oxygen-dependent manner, the activity of its C-terminal domain on the degradation of Sre1N, we tested the role of the respective deletions of the Tpa1_N and Tpa1_C domains on stop codon readthrough. Both Tpa1 domains are required for translation termination to occur at a wild type level (Fig. 3*C*). Finally, in *S. pombe*, Nro1 was shown to interact with Ofd1, leading to the inhibition of its effect on Sre1N degradation (23). Interestingly, large scale comprehensive purification in yeast *S. cerevisiae* using TAP purification identified the Nro1 homolog (Yor051c) as a Tpa1 partner (28). Disruption of the *YOR051C/ETT1* gene results in increased readthrough of stop codons present in the luciferase and *ade1-14* reporters compared with wild type cells. Yet this effect is quantitatively less important than the one observed in *tpa1*Δ strains. In addition, the combined deletion of both *TPA1* and *ETT1* genes did not further diminish translation termination efficiency compared with individual deletions, supporting a concomitant action. These data support the idea that Ett1 and Tpa1 act in the same pathway in *S. cerevisiae*. The involvement of Tpa1 in correct translation termination sustains co-immunoprecipitation results, showing that Tpa1 interacts with translation termination factors eRF1 and eRF3 as well as with poly(A) binding protein Pab1 in *S. cerevisiae* (18). Tpa1 is very likely to be a prolyl-4-hydroxylase acting as an oxygen sensor (52), and the integrity of its active site is crucial to reduce stop codon readthrough. Therefore, we suspect that in the presence of oxygen, Tpa1 hydroxylates a proline residue in a specific target protein(s). Because it needs dioxygen as co-substrate, Tpa1 should be unable to hydroxylate its substrate during hypoxia. As a consequence, this could increase the level of inaccurate translation termination. Whether Tpa1 affects readthrough by directly modifying eRF1, eRF3, or Pab1 or another protein controlling these factors remains to be investigated. However, consistent with the results reported by Bedwell

and co-workers (18), we observed that stop codon suppression still occurred both in *PSI*⁺ and *PSI*⁻ strains, indicating that it does not occur through control of eRF3 aggregation.

Ett1, the *S. cerevisiae* Nro1 ortholog, has been identified in a genetic-wide screen aimed at identifying genes from *S. cerevisiae* that affect replication of a positive-strand RNA virus (Brome mosaic virus (BMV)) (59). Among the nearly 100 genes whose deletion either enhanced or reduced viral replication, many are involved in transcription, RNA processing, translation, and protein degradation. Deletion of *ETT1* gene resulted in enhancement of viral replication, suggesting that Ett1 inhibits replication. This is not the first time that proteins from yeast, but also human, are identified to affect both RNA virus replication and translation. This is for instance the case for yeast proteins Pat1, Lsm1, and Lsm6, functioning in mRNA decapping. These proteins are involved in BMV RNA translation and are recruited from translation complexes to RNA replication complexes (60, 61). Similarly, in human cells, translation and replication of hepatitis C virus RNA depends on Pat1, Rck/P54 (Dhh1 in yeast), and the Lsm1–7 complex (62). However, it remains to be determined whether or not there is a functional link between the roles of Ett1 in inhibition of BMV replication and in enhancement of stop codon recognition or whether the effect of Ett1 on BMV results from altered termination of translation of a specific BMV replication factor.

Tpa1 Is Involved in Regulation of Hap1 Transcription Factor Activity—The precise identification of the cellular function of Tpa1 is complicated by the observation that the orthologous Ofd1 is implicated in an apparently completely different process, *i.e.* the oxygen-dependent regulation of Sre1, the fission yeast (or SREBP (22)). The *S. pombe* SREBP transcription factor is anchored at the endoplasmic reticulum membrane, but upon sterol depletion it is cleaved, and its N-terminal domain enters the nucleus to activate transcription of genes encoding sterol biosynthesis enzymes, as observed for its mammalian counterpart (24, 27). In addition, in response to low oxygen levels, Sre1 stimulates transcription of genes required for adaptation to hypoxia. In budding yeast, several transcription factors (Upc2, Ecm22, Mga2, Hap1, Rox1, ...) have been implicated in the response to sterol depletion and/or hypoxia, but none present significant sequence homology with members of the SREBP family (57, 58, 63, 64). We have, therefore, investigated the effect of the deletion of *TPA1* on genes controlled by Mga2 and Hap1 as representative of transcription factors affecting the response to oxygen concentration. Mga2 is an endoplasmic reticulum membrane protein activated during hypoxia by processing of the full-length protein into a smaller soluble transcription factor domain that is addressed to the nucleus similarly to *S. pombe* Sre1 and mammalian SREBP (57, 64, 65). Hap1 is a transcription factor involved in the complex regulation of gene expression in response to levels of heme and oxygen (66, 67). Our choice to study Hap1 was also motivated by the observation that the deletion of *TPA1* gene was shown to rescue the synthetic lethality phenotype of a $\Delta hap1 \Delta upc2 \Delta ecm22$ triple mutant (68).

No effect of the deletion of *TPA1* on the expression of reporters regulated by the Mga2 transcription factor was detected (data not shown). In contrast, deletion of *TPA1*

generated significant changes (4-fold increase) in transcription of two reporters driven by the *CYC1* UAS1 or the *CYB2* UAS1 (Fig. 5). Expression of both *CYC1* and *CYB2* is stimulated by these sequences in the presence of oxygen through the Hap1 transcription factor (69–71). Our analysis, therefore, suggests that Tpa1 represses specifically Hap1 activity by an unknown mechanism.

The functional link between Tpa1 and Hap1 is reminiscent of that between Ofd1 and Sre1N (22). Interestingly, another prolyl-4-hydroxylase, human PHD2, has been implicated in the control of the activity of a family of transcription factors; that is, HIF, by hydroxylation of conserved proline residues that targets HIF factors to ubiquitin-mediated degradation (for review, see Ref. 72). We have experimental evidence that in *S. cerevisiae*, Tpa1 also influences the activity of a transcription factor, Hap1. Hap1 is structurally unrelated to SREBPs and HIF. However, Hap1 is degraded into smaller fragments in the absence of oxygen, whereas only the unprocessed form is observed in the presence of oxygen (58). We have observed that Tpa1 represses the activity of Hap1 (Fig. 5). Tpa1 functions very likely as an oxygen sensor through its N-terminal PHD domain, but the role of Tpa1 in modulating the activity of Hap1 remains to be clarified.

Conclusion—The resolution of the crystal structure of Tpa1 revealed that this protein contains two DSBH domains and that it is a putative prolyl-4-hydroxylase whose active site is located in its N-terminal domain. Tpa1 probably acts as an oxygen sensor system, and our genetic experiments show that it is involved in two unrelated cellular processes. First, Tpa1 reduces stop codon readthrough, and its enzymatic activity is critical for this function. Second, Tpa1 participates in the regulation of the transcription of genes by the Hap1 transcription factor and represses Hap1. Whether the implication of Tpa1 in these two pathways is mediated by a unique substrate protein that will further act on distinct proteins involved in these two processes or by at least two substrates implicated in each process remains to be elucidated.

Acknowledgments—We are indebted to K. Blondeau for help with *SeMet* labeling and V. Henriot, B. Bonneau, and D. Rentz for general work including competent cells, cloning, minipreps, and media. We thank D. M. Bedwell, C. E. Martin, M. Globerg, and B. Guiard for plasmids and yeast strains.

Note Added in Proof—While we were finalizing this article, the crystal structure of *S. cerevisiae* was described by Kim *et al.* ((2010) *Nucleic Acids Res.* **38**, 2099–2110). In addition to the structure of the protein in a binary complex with Fe(III), they solved the structure of a ternary complex with Fe(III) and 2OG. No significant differences exist between all these structures. These authors also present results on poly(rA) binding by Tpa1.

REFERENCES

1. Gallie, D. R. (1991) *Genes Dev.* **5**, 2108–2116
2. Pestova, T., Lorsch, J. R., and Hellen, C. U. T. (2007) in *Translational Control in Biology and Medicine* (Mathews, M. B., Sonenberg, N., and Hershey, J. W. B., eds) pp 87–128, Cold Spring Harbor Laboratory Press, Cold Spring Harbor, NY
3. Frolova, L., Le Goff, X., Rasmussen, H. H., Cheperegin, S., Drugeon, G., Kress, M., Arman, I., Haenni, A. L., Celis, J. E., and Philippe, M. (1994) *Nature* **372**, 701–703
4. Kisselev, L. L., and Buckingham, R. H. (2000) *Trends Biochem. Sci.* **25**,

Structural and Functional Study of Tpa1, an O₂ Sensor

- 561–566
5. Kisselev, L., Ehrenberg, M., and Frolova, L. (2003) *EMBO J.* **22**, 175–182
 6. Alkalaeva, E. Z., Pisarev, A. V., Frolova, L. Y., Kisselev, L. L., and Pestova, T. V. (2006) *Cell* **125**, 1125–1136
 7. Stansfield, I., Jones, K. M., Kushnirov, V. V., Dagkesamanskaya, A. R., Poznyakovski, A. I., Paushkin, S. V., Nierras, C. R., Cox, B. S., Ter-Avanesyan, M. D., and Tuite, M. F. (1995) *EMBO J.* **14**, 4365–4373
 8. Zhouravleva, G., Frolova, L., Le Goff, X., Le Guellec, R., Inge-Vechtomov, S., Kisselev, L., and Philippe, M. (1995) *EMBO J.* **14**, 4065–4072
 9. Frolova, L., Le Goff, X., Zhouravleva, G., Davydova, E., Philippe, M., and Kisselev, L. (1996) *RNA* **2**, 334–341
 10. Bonetti, B., Fu, L., Moon, J., and Bedwell, D. M. (1995) *J. Mol. Biol.* **251**, 334–345
 11. von der Haar, T., and Tuite, M. F. (2007) *Trends Microbiol.* **15**, 78–86
 12. Amrani, N., Ganesan, R., Kervestin, S., Mangus, D. A., Ghosh, S., and Jacobson, A. (2004) *Nature* **432**, 112–118
 13. Cosson, B., Couturier, A., Chabelskaya, S., Kiktev, D., Inge-Vechtomov, S., Philippe, M., and Zhouravleva, G. (2002) *Mol. Cell. Biol.* **22**, 3301–3315
 14. Graille, M., Heurgué-Hamard, V., Champ, S., Mora, L., Scrima, N., Ulryck, N., van Tilbeurgh, H., and Buckingham, R. H. (2005) *Mol. Cell* **20**, 917–927
 15. Heurgué-Hamard, V., Champ, S., Engström, A., Ehrenberg, M., and Buckingham, R. H. (2002) *EMBO J.* **21**, 769–778
 16. Heurgué-Hamard, V., Graille, M., Scrima, N., Ulryck, N., Champ, S., van Tilbeurgh, H., and Buckingham, R. H. (2006) *J. Biol. Chem.* **281**, 36140–36148
 17. Mora, L., Heurgué-Hamard, V., de Zamaroczy, M., Kervestin, S., and Buckingham, R. H. (2007) *J. Biol. Chem.* **282**, 35638–35645
 18. Keeling, K. M., Salas-Marco, J., Osherovich, L. Z., and Bedwell, D. M. (2006) *Mol. Cell. Biol.* **26**, 5237–5248
 19. Aravind, L., and Koonin, E. V. (2001) *Genome Biol* **2**, RESEARCH0007
 20. Chang, B., Chen, Y., Zhao, Y., and Bruick, R. K. (2007) *Science* **318**, 444–447
 21. Clifton, I. J., McDonough, M. A., Ehrismann, D., Kershaw, N. J., Granatino, N., and Schofield, C. J. (2006) *J. Inorg. Biochem.* **100**, 644–669
 22. Hughes, B. T., and Espenshade, P. J. (2008) *EMBO J.* **27**, 1491–1501
 23. Lee, C. Y., Stewart, E. V., Hughes, B. T., and Espenshade, P. J. (2009) *EMBO J.* **28**, 135–143
 24. Espenshade, P. J., and Hughes, A. L. (2007) *Annu. Rev. Genet.* **41**, 401–427
 25. Todd, B. L., Stewart, E. V., Burg, J. S., Hughes, A. L., and Espenshade, P. J. (2006) *Mol. Cell. Biol.* **26**, 2817–2831
 26. Hughes, A. L., Lee, C. Y., Bien, C. M., and Espenshade, P. J. (2007) *J. Biol. Chem.* **282**, 24388–24396
 27. Hughes, A. L., Todd, B. L., and Espenshade, P. J. (2005) *Cell* **120**, 831–842
 28. Krogan, N. J., Cagney, G., Yu, H., Zhong, G., Guo, X., Ignatchenko, A., Li, J., Pu, S., Datta, N., Tikuisis, A. P., Punna, T., Peregrín-Alvarez, J. M., Shales, M., Zhang, X., Davey, M., Robinson, M. D., Paccanaro, A., Bray, J. E., Sheung, A., Beattie, B., Richards, D. P., Canadien, V., Lalev, A., Mena, E., Wong, P., Starostine, A., Canete, M. M., Vlasblom, J., Wu, S., Orsi, C., Collins, S. R., Chandran, S., Haw, R., Rilstone, J. J., Gandi, K., Thompson, N. J., Musso, G., St Onge, P., Ghanny, S., Lam, M. H., Butland, G., Altaf-Ul, A. M., Kanaya, S., Shilatifard, A., O’Shea, E., Weissman, J. S., Ingles, C. J., Hughes, T. R., Parkinson, J., Gerstein, M., Wodak, S. J., Emili, A., and Greenblatt, J. F. (2006) *Nature* **440**, 637–643
 29. Hendrickson, W. A., Horton, J. R., and LeMaster, D. M. (1990) *EMBO J.* **9**, 1665–1672
 30. Kabsch, W. (1993) *J. Appl. Crystallogr.* **26**, 795–800
 31. Schneider, T. R., and Sheldrick, G. M. (2002) *Acta Crystallogr. D Biol. Crystallogr.* **58**, 1772–1779
 32. Bricogne, G., Vornrhein, C., Flensburg, C., Schiltz, M., and Paciorek, W. (2003) *Acta Crystallogr. D Biol. Crystallogr.* **59**, 2023–2030
 33. Terwilliger, T. C. (1999) *Acta Crystallogr. D Biol. Crystallogr.* **55**, 1863–1871
 34. Cowtan, K. (2006) *Acta Crystallogr. D Biol. Crystallogr.* **62**, 1002–1011
 35. Emsley, P., and Cowtan, K. (2004) *Acta Crystallogr. D Biol. Crystallogr.* **60**, 2126–2132
 36. Adams, P. D., Grosse-Kunstleve, R. W., Hung, L. W., Ioerger, T. R., McCoy, A. J., Moriarty, N. W., Read, R. J., Sacchettini, J. C., Sauter, N. K., and Terwilliger, T. C. (2002) *Acta Crystallogr. D Biol. Crystallogr.* **58**, 1948–1954
 37. Vagin, A., and Teplyakov, A. (1997) *J. Appl. Crystallogr.* **30**, 1022–1025
 38. Eaglestone, S. S., Ruddock, L. W., Cox, B. S., and Tuite, M. F. (2000) *Proc. Natl. Acad. Sci. U.S.A.* **97**, 240–244
 39. Christianson, T. W., Sikorski, R. S., Dante, M., Shero, J. H., and Hieter, P. (1992) *Gene* **110**, 119–122
 40. Ramil, E., Agrimonti, C., Shechter, E., Gervais, M., and Guiard, B. (2000) *Mol. Microbiol.* **37**, 1116–1132
 41. Dziembowski, A., Ventura, A. P., Rutz, B., Caspary, F., Faux, C., Halgand, F., Laprèvote, O., and Séraphin, B. (2004) *EMBO J.* **23**, 4847–4856
 42. Kushnirov, V. V. (2000) *Yeast* **16**, 857–860
 43. Hausinger, R. P. (2004) *Crit. Rev. Biochem. Mol. Biol.* **39**, 21–68
 44. McDonough, M. A., Li, V., Flashman, E., Chowdhury, R., Mohr, C., Liénard, B. M., Zondlo, J., Oldham, N. J., Clifton, I. J., Lewis, J., McNeill, L. A., Kurzeja, R. J., Hewitson, K. S., Yang, E., Jordan, S., Syed, R. S., and Schofield, C. J. (2006) *Proc. Natl. Acad. Sci. U.S.A.* **103**, 9814–9819
 45. Albuquerque, C. P., Smolka, M. B., Payne, S. H., Bafna, V., Eng, J., and Zhou, H. (2008) *Mol. Cell. Proteomics* **7**, 1389–1396
 46. Cleasby, A., Wonacott, A., Skarzynski, T., Hubbard, R. E., Davies, G. J., Proudfoot, A. E., Bernard, A. R., Payton, M. A., and Wells, T. N. (1996) *Nat. Struct. Biol.* **3**, 470–479
 47. Just, V. J., Stevenson, C. E., Bowater, L., Tanner, A., Lawson, D. M., and Bornemann, S. (2004) *J. Biol. Chem.* **279**, 19867–19874
 48. Steiner, R. A., Kalk, K. H., and Dijkstra, B. W. (2002) *Proc. Natl. Acad. Sci. U.S.A.* **99**, 16625–16630
 49. Pang, H., Bartlam, M., Zeng, Q., Miyatake, H., Hisano, T., Miki, K., Wong, L. L., Gao, G. F., and Rao, Z. (2004) *J. Biol. Chem.* **279**, 1491–1498
 50. Cassab, G. I. (1998) *Annu. Rev. Plant Physiol. Plant Mol. Biol.* **49**, 281–309
 51. Myllyharju, J. (2003) *Matrix Biol.* **22**, 15–24
 52. Schofield, C. J., and Ratcliffe, P. J. (2004) *Nat. Rev. Mol. Cell Biol.* **5**, 343–354
 53. Koski, M. K., Hieta, R., Hirsilä, M., Rönkä, A., Myllyharju, J., and Wierenga, R. K. (2009) *J. Biol. Chem.* **284**, 25290–25301
 54. Chowdhury, R., McDonough, M. A., Mecinović, J., Loenarz, C., Flashman, E., Hewitson, K. S., Domene, C., and Schofield, C. J. (2009) *Structure* **17**, 981–989
 55. Sundheim, O., Vågbo, C. B., Bjørås, M., Sousa, M. M., Talstad, V., Aas, P. A., Drabløs, F., Krokan, H. E., Tainer, J. A., and Slupphaug, G. (2006) *EMBO J.* **25**, 3389–3397
 56. Puig, O., Caspary, F., Rigaut, G., Rutz, B., Bouveret, E., Bragado-Nilsson, E., Wilm, M., and Séraphin, B. (2001) *Methods* **24**, 218–229
 57. Jiang, Y., Vasconcelles, M. J., Wretzel, S., Light, A., Martin, C. E., and Goldberg, M. A. (2001) *Mol. Cell. Biol.* **21**, 6161–6169
 58. Hon, T., Dodd, A., Dirmeier, R., Gorman, N., Sinclair, P. R., Zhang, L., and Poyton, R. O. (2003) *J. Biol. Chem.* **278**, 50771–50780
 59. Kushner, D. B., Lindenbach, B. D., Grdzlishvili, V. Z., Noueiry, A. O., Paul, S. M., and Ahlquist, P. (2003) *Proc. Natl. Acad. Sci. U.S.A.* **100**, 15764–15769
 60. Díez, J., Ishikawa, M., Kaido, M., and Ahlquist, P. (2000) *Proc. Natl. Acad. Sci. U.S.A.* **97**, 3913–3918
 61. Noueiry, A. O., Díez, J., Falk, S. P., Chen, J., and Ahlquist, P. (2003) *Mol. Cell. Biol.* **23**, 4094–4106
 62. Scheller, N., Mina, L. B., Galão, R. P., Chari, A., Giménez-Barcons, M., Noueiry, A., Fischer, U., Meyerhans, A., and Díez, J. (2009) *Proc. Natl. Acad. Sci. U.S.A.* **106**, 13517–13522
 63. Davies, B. S., and Rine, J. (2006) *Genetics* **174**, 191–201
 64. Hoppe, T., Matuschewski, K., Rape, M., Schlenker, S., Ulrich, H. D., and Jentsch, S. (2000) *Cell* **102**, 577–586
 65. Jiang, Y., Vasconcelles, M. J., Wretzel, S., Light, A., Gilooly, L., McDaid, K., Oh, C. S., Martin, C. E., and Goldberg, M. A. (2002) *Eukaryot. Cell* **1**, 481–490
 66. Pfeifer, K., Kim, K. S., Kogan, S., and Guarente, L. (1989) *Cell* **56**, 291–301
 67. Zhang, L., and Hach, A. (1999) *Cell. Mol. Life Sci.* **56**, 415–426
 68. Valachovic, M., Bareither, B. M., Shah Alam Bhuiyan, M., Eckstein, J., Barbuch, R., Balderes, D., Wilcox, L., Sturley, S. L., Dickson, R. C., and Bard, M. (2006) *Genetics* **173**, 1893–1908
 69. Lodi, T., and Guiard, B. (1991) *Mol. Cell. Biol.* **11**, 3762–3772
 70. Pfeifer, K., Arcangioli, B., and Guarente, L. (1987) *Cell* **49**, 9–18
 71. Pfeifer, K., Prezant, T., and Guarente, L. (1987) *Cell* **49**, 19–27
 72. Kaelin, W. G. (2005) *Annu. Rev. Biochem.* **74**, 115–128

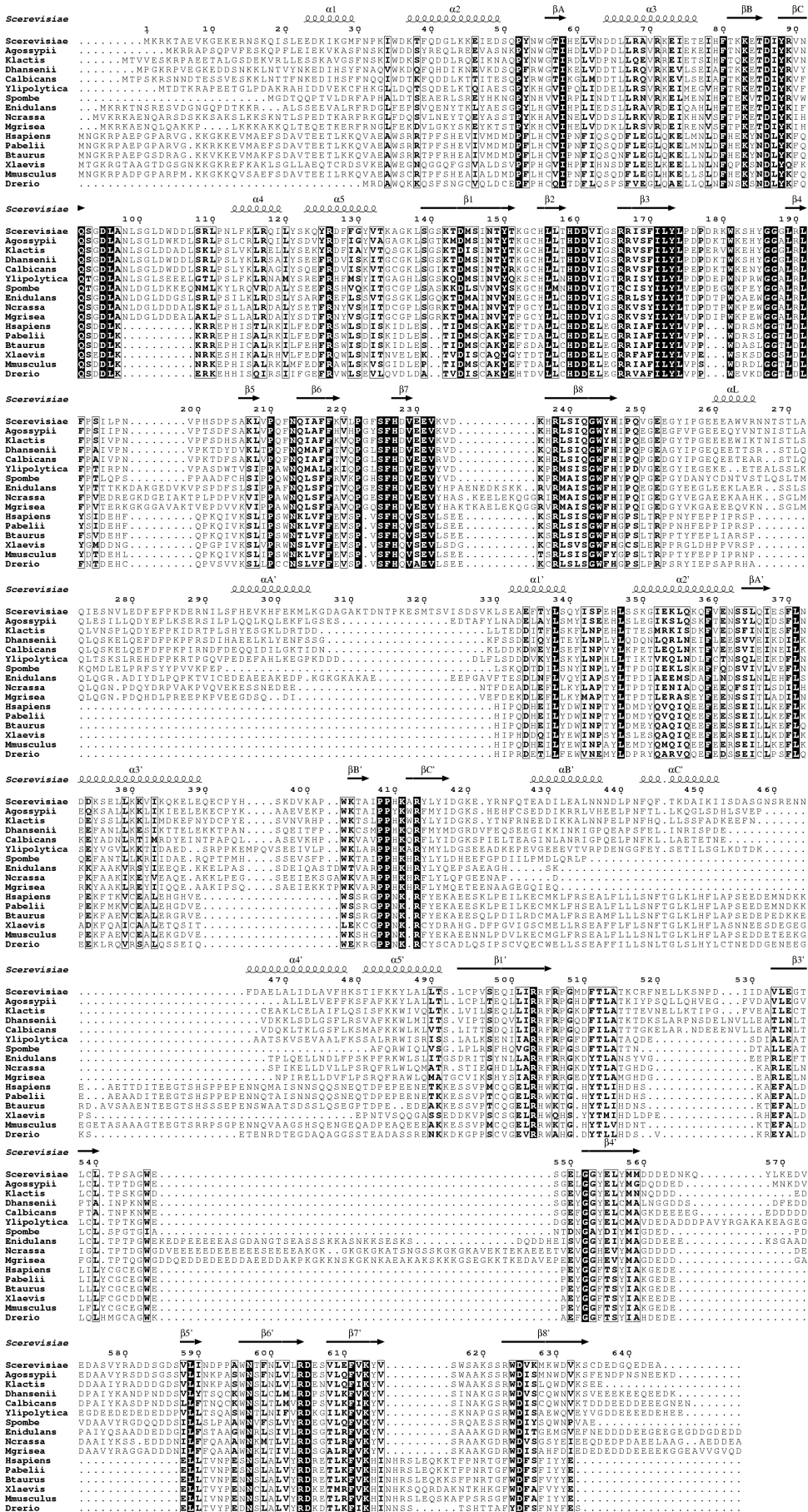
Supplementary Table 1: Oligonucleotides used in this study

Name	Sequence
OBS2151	GGCGGTCTCTCCGGATCATAAAGGAGGATATATATGCATCACCATCACCATCACATGA AGAGAAAAACTGCTGAAG
OBS2152	GCCTCCGGAGAGACCTTACGCTTCATCTTCCTGAC
OBS3527	GCGCGGATCCCAGTAATTTTTCTTCTCACG
OBS3528	GCGCGCGGCCGCGGCATTTTCATAGTTCTGTCTGT
OBS3687	AAAGGGATGTCACCTTGTGACTGCTGATAACGTTATTGGCTCTAGAAGGATTA
OBS3688	TAATCCTTCTAGAGCCAATAACGTTATCAGCAGTCAACAAGTGACATCCCTTT
OBS3738	TGTGTTGTTACGGACCCACGCTTC
OBS3739	GAAGCGTGGGTCCGTAACAACACATAAACAATTAACCCGTCTTATTAAG
OBS3740	TCCACTTTGGCGCAGATTGAATC
OBS3741	GATTCAATCTGCGCCAAAGTGGACATTATATTTCCCGGTATATTTGGTG
OBS3822	GATGTCAAATCATGTGATGAAGATGGTCAGGAAGATGAAGCGTCCATGGAAAAGAG AAG
OBS3823	AATATCTAAGCTGCCATTTACTTAATAAGACGGGTTAATTGTTACGACTCACTATAG GG
OBS3824	TACATACCTGGTGAAGAAGAAGCGTGGGTCCGTAACAACACATCCATGGAAAAGAG AAG
OBS3831	CGCTTCATCTTCTGACCATCTTCATCACATGATTTGACATC
OBS3832	TGTGTTGTTACGGACCCACGCTTCTTCTTACCAGGTATGTA
OBS3844	ACAATTAACCCGTCTTATTAAGTAAATGGCAGCTTAGATATT
OBS3866	TGAAGAAAAAAGGAGAACAGTCCAAGAAAGTAATCGTACAGAACACAGGAAACAG CTATGACC
OBS3867	GGCAACAGAAGGAGTGAGTAAAAATAAAAAAGAAGCGTGGATGCGCGTTGTAAAA CGACGGCCAGT

Legend to figure S1. Multiple sequence alignment of Tpa1

Eukaryotic orthologs of Tpa1 were aligned using ClustalW. Strictly conserved residues are in white on a black background. Partially conserved amino acids are boxed. Secondary structure elements assigned from the *S. cerevisiae* Tpa1 structure are indicated above the alignment.

Figure S1.



Legend to figure S2. Effect of *Tpa1* deletion, catalytic site mutation and truncation on suppression of *ade1-14*

Equivalent number of cells of the yeast strains of the indicated genotype were grown on media lacking tryptophan (to select for the plasmid) and on media lacking tryptophan and adenine for 3 days at 30°C. (Using this strain, at this time point, suppression of the *ade1-14* mutation by [*PSI*⁺] on this media was sufficiently limited to allow scoring of the suppression of *ade1-14* resulting from the deletion of *TPA1*.) Enhanced readthrough of the UGA stop codon present in the *ade1-14* allele in strain lacking *TPA1* compared to wild type is indicated by the lower accumulation of the red pigment on media lacking tryptophan and enhanced growth on media lacking tryptophan and adenine. This effect is suppressed by a plasmid encoding wild-type *TPA1* but not a catalytic site mutant thereof, nor plasmids expressing only the N- or C-terminal domain of the protein. The residual growth of the *tpa1Δ* strain carrying a plasmid-borne wild type *TPA1* allele compared to the isogenic wild type control on media lacking tryptophan and adenine is attributed to the small fraction of cells having lost the *TPA1* plasmid.

Figure S2.

